Supporting Information

Interface Modulating CNTs@PANi Hybrids by Controlled Unzipping of the Walls of CNTs to Achieve Tunable High-Performance Microwave Absorption

Huagao Wang, Fanbin Meng*, Fei Huang, Changfei Jing, Ying Li, Wei Wei and Zuowan Zhou*

Key Laboratory of Advanced Technologies of Materials (Ministry of Education), School of Materials Science and Engineering, Southwest Jiaotong University, Chengdu 610031, P. R. China

Corresponding Author

E-mail: mengfanbin_wing@126.com (Fanbin Meng)

zwzhou@swjtu.edu.cn (Zuowan Zhou)

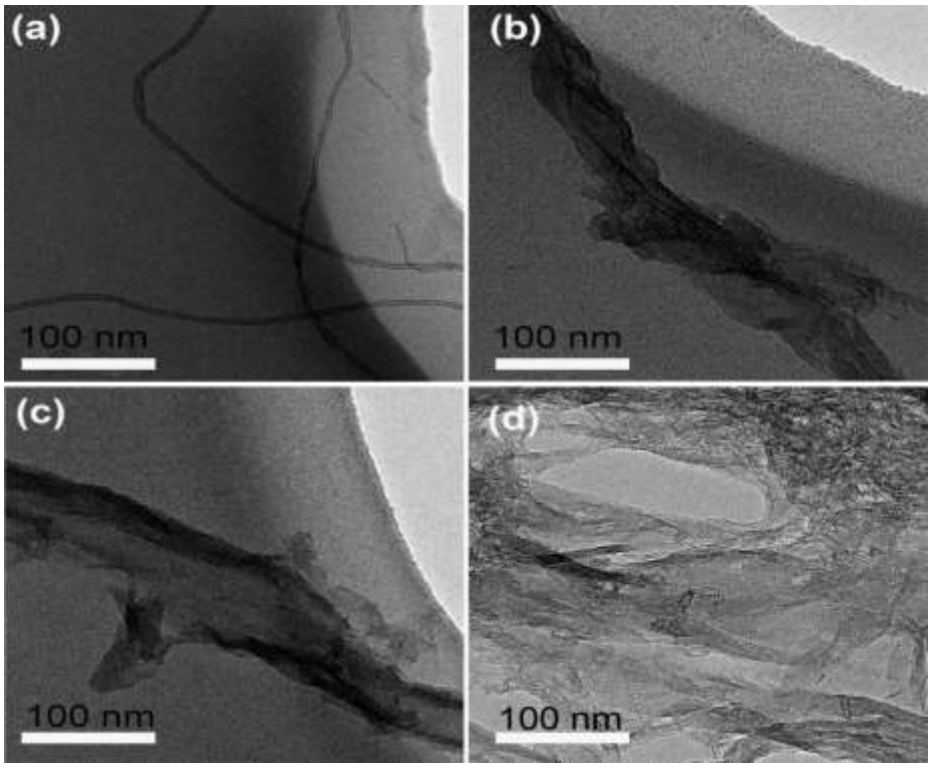

Figure S1. TEM images of the all the op-CNTs：(a) 0CNTs, (b) 2CNTs, (c) 4CNTs and (d) 6CNTs.

X-ray diffraction (XRD) patterns were firstly carried out to investigate the structures of the op-CNTs. As depicted in **Figure S2**, the strongest and sharpest diffraction peak of the 0CNTs located at 25.8^{o} is attributed to the (002) plane of graphite. However, it is clearly found that the peaks become much broader after treated by permanganate in acid, suggesting that the introduction of oxygen atoms destroy the p-conjugated network and lead the incompact stacking of the peeled graphene nanosheets in the 2CNTs, 4CNTs and 6CNTs. Meanwhile, the diffraction peak of 2CNTs, 4CNTs and 6CNTs shifts to the lower angle compared with the 0CNTs, indicating the CNTs were unzipped to form CNTs bridged with graphene oxide nanosheets and graphene nanosheets, respectively.[1-4]

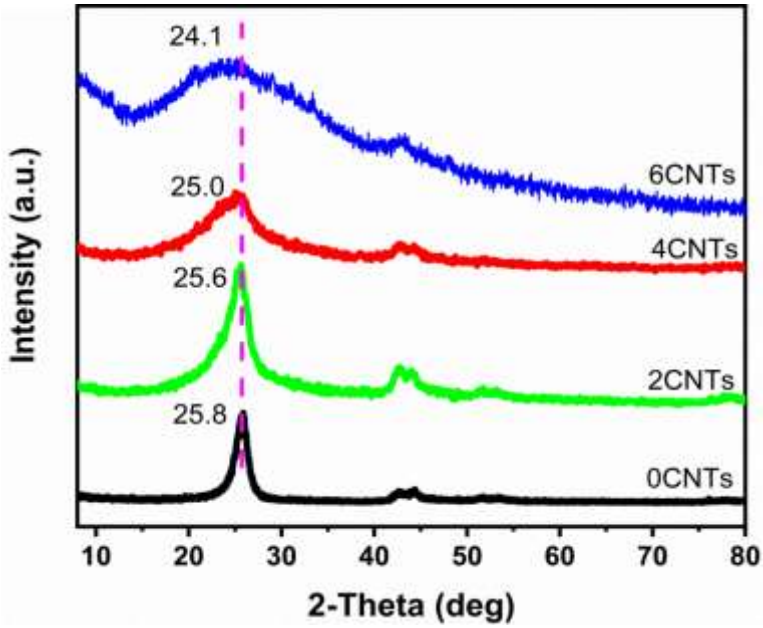

Figure S2. XRD patterns of the 0CNTs, 2CNTs, and 4CNTs and 6CNTs.

Raman spectroscopy was also conducted on to investigate the partial or complete peeled CNTs. **Figure S3** depicts the pristine CNTs and the peeled CNTs, it is notably seen that there are two predominant peaks located at ~1340 and ~1580 cm^{-1}, which was attributed to the D and G bands, respectively. However, with the increase of oxidative peeled period, the corresponding peaks of D bands shift towards to the high wavenumbers compared with the 0CNTs, (1580 cm^{-1} for 0CNTs, 1602 cm^{-1} for 2CNTs, 1606 cm^{-1} for 4CNTs and 1598 cm^{-1} for 6CNTs), suggesting that some oxygen-containing functional groups have been introduced.[5] Meanwhile, after the CNTs were oxidation peeling treatment, the ratios of I_D to I_G increased from 1.05 to 1.18 higher that of pristine CNTs, indicating that an increasing in the degree of disorder occurred after oxidation peeled treatment and thus result in introducing some defect sites. [3, 6]

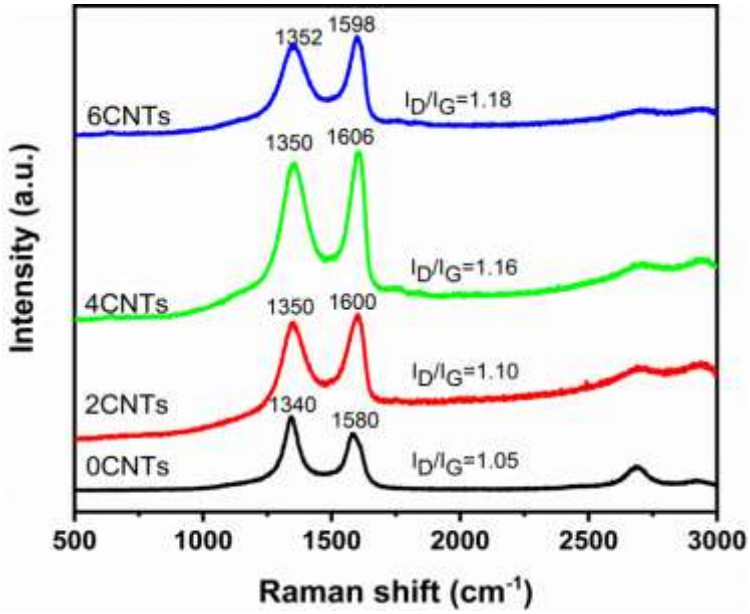

Figure S3. Raman spectra of the 0CNTs, 2CNTs, and 4CNTs and 6CNTs.

For further demonstrate the functional groups in the treated CNTs, the FT-IR is shown in **Figure S4**. As can be seen, the peak observed at about 1630 cm^{-1} is ascribed to C=C bond.[3] After the CNTs were oxidative peeled, a shoulder peak at around 1730 cm^{-1} was introduced, corresponding the stretching mode of –C=O, which indicate that various carboxyl and hydroxyl functionalities were existed on the as-prepared oxidation peeled CNTs. In addition, a broad peak appears at 3400 cm^{-1} on the 0CNTs implies that they were introduced during the proprietary production or purification (manufacturing) processes.[7] The results suggested some oxygen-containing functional groups and defect sites were produced. The above findings confirm the successful preparation of partial and complete peeled CNTs.

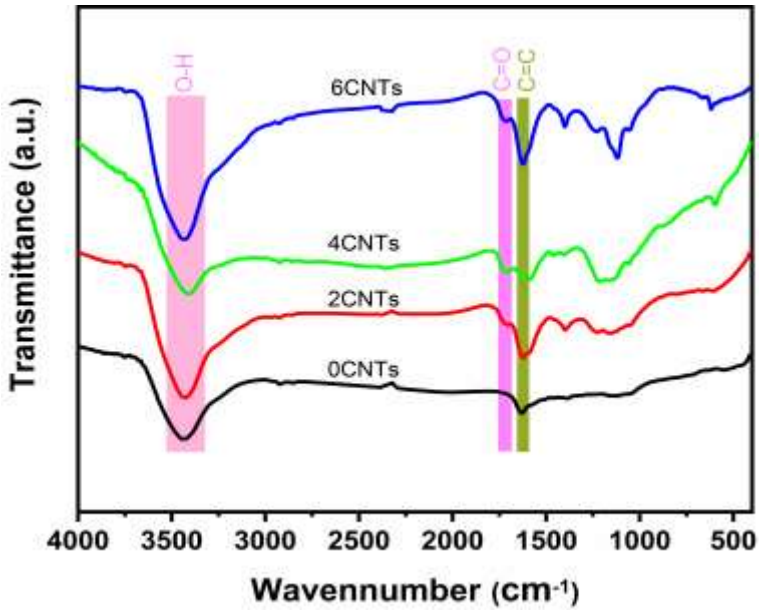

Figure S4. FT-IR spectra of the 0CNTs, 2CNTs, 4CNTs, and 6CNTs.

The mechanism of CNTs opening is based on the oxidation of alkenes by permanganate in acid. As previously reported,[8-10] manganate ester is formed firstly as the rate-determining (**Scheme S**1, **step 2**), and further oxidation is possible to afford the dione in the dehydrating medium (**step 3**). Juxtaposition of the buttressing ketones distorts the β,γ-alkenes, making them more prone to the next attack by permanganate. As the oxidation time increases, the buttressing-induced strain on the β,γ-alkenes lessens because there is more space for carbonyl projection; while, the bond-angle strain induced by the enlarging hole (or tear if generating from the end of the carbon nanotube) would make the β,γ-alkenes (**step 4**) uninitiated site on the same tube. The ketones can be further converted, through their O-protonated forms, to the carboxylic acids that will line edges of the nanoribbons. Finally, relief of the bond-angle strain when the carbon nanotubes opens to the graphene nanoribbon slows further dione formation and cutting (**step 5**).

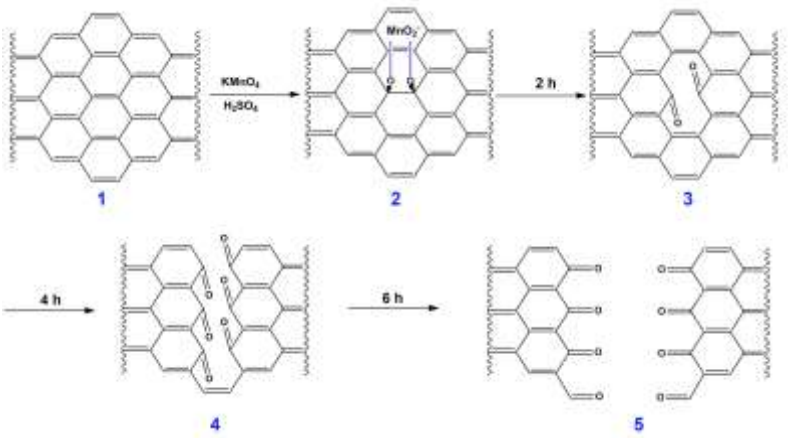

Scheme S1. The proposed chemical mechanism of CNTs unzipping.

In order to evaluate the defect degree of CNTs@PANi hybrids, the Raman spectroscopy is processed by peak fitting. The results demonstrate that the defect degree the CNTs@PANi is enhanced from 1.44 to 2.35 for the 0CNTs@PANi, 2CNTs@PANi, 4CNTs@PANi and 6CNTs@PANi, respectively.

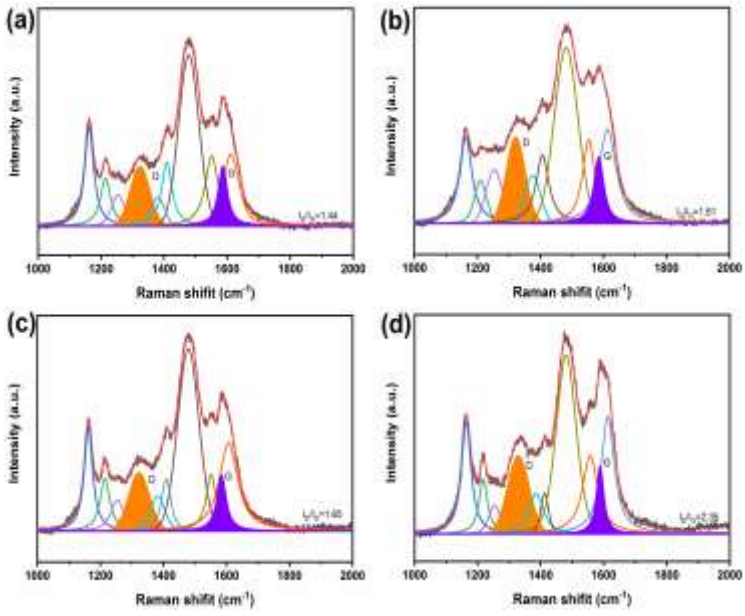

Figure S5. The peak fitting results of the Raman spectroscopy for CNTs@PANi: (a) 0CNTs@PANi, (b) 2CNTs@PANi, (c) 4CNTs@PANi and (d) 6CNTs@PANi.

In addition, **Figure S6** also displays the TGA curves of 0CNTs@ PANi, 2CNTs@

PANi and 4CNTs@ PANi and 6CNTs@ PANi. It can be found that the final weight loss of the oxidation peeled CNTs@PANi hybrids was increased as prolong the oxidation peeled period, indicating the amount of PANi increased, which is corresponding to the XPS analysis.

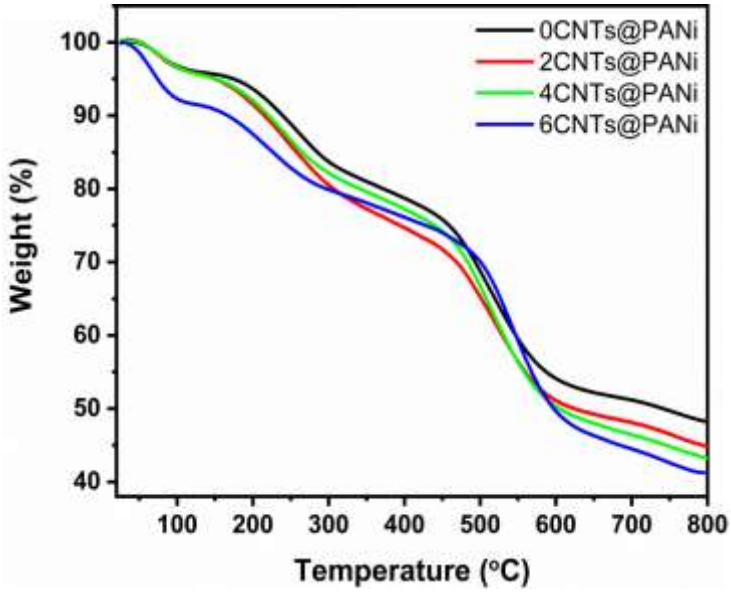

Figure S6. TG curves of 0CNTs@PANi, 2CNTs@PANi, 4CNTs@PANi and 6CNTs@PANi.

Reference

(1) Ye, M.; Hu, C.; Lv, L.; Qu, L. Graphene-Winged Carbon Nanotubes as High-Herformance Lithium-Ion Batteries Anode with Super-Long Cycle Life. *J. Power Sources* **2016**, *305*, 106-114.

(2) Chen, L.; Xu, C.; Du, R.; Mao, Y.; Xue, C.; Chen, L.; Qu, L.; Zhang, J.; Yi, T. Rational Design of Three-Dimensional Nitrogen-Doped Carbon Nanoleaf Networks for High-Performance Oxygen Reduction. *J. Mater. Chem. A* **2015**, *3* (10), 5617-5627.

(3) Li, Y. S.; Liao, J. L.; Wang, S. Y.; Chiang, W. H. Intercalation-Assisted Longitudinal

Unzipping of Carbon Nanotubes for Green and Scalable Synthesis of Graphene Nanoribbons. *Sci. Rep.* **2016**, *6*, 22755.

(4) Yang, Z.; Liu, M.; Zhang, C.; Tjiu, W. W.; Liu, T.; Peng, H. Carbon Nanotubes Bridged with Graphene Nanoribbons and Their Use in High-Efficiency Dye-Sensitized Solar Cells. *Angew Chem. Int. Ed. Engl.* **2013**, *52* (14), 3996-9.

(5) Rao, A. M.; Eklund, P. C.; Bandow, S.; Thess, A.; Smalley, R. E. Evidence for Charge Transfer in Doped Carbon Nanotube Bundles from Raman Scattering. *Nature* **1997**, *388*, 257-259.

(6) Zhao, Z.; Yang, Z.; Hu, Y.; Li, J.; Fan, X. Multiple Functionalization of Multi-Walled Carbon Nanotubes with Carboxyl and Amino groups. *Appl. Surf. Sci.* **2013**, *276*, 476-481.

(7) Avilés, F.; Cauich-Rodríguez, J. V.; Moo-Tah, L.; May-Pat, A.; Vargas-Coronado, R. Evaluation of Mild Acid Oxidation Treatments for MWCNT Functionalization. *Carbon* **2009**, *47* (13), 2970-2975.

(8) Kosynkin, D. V.; Higginbotham, A. L.; Alexander, S.; Lomeda, J. R.; Ayrat, D.; B Katherine, P.; Tour, J. M. Longitudinal Unzipping of Carbon Nanotubes to form Graphene Nanoribbons. *Nature* **2017**, *458* (7240), 872-876.

(9) Higginbotham, A. L.; Kosynkin, D. V.; Sinitskii, A.; Sun, Z.; Tour, J. M. Lower-Defect Gphene Oxide Nanoribbons from Multiwalled Carbon Nanotubes. *ACS. Nano* **2010**, *4* (4), 2059-2069.

(10) Cataldo, F.; Compagnini, G.; Patané, G.; Ursini, O.; Angelini, G.; Ribic, P. R.; Margaritondo, G.; Cricenti, A.; Palleschi, G.; Valentini, F. Graphene Nanoribbons

Produced by the Oxidative Unzipping of Single-Wall Carbon Nanotubes. *Carbon* **2010**, *48* (9), 2596-2602.

Appendix:

For competition of both relaxation and conductance losses, Non-linear least squares fitting method is applied to fit a curve. According to this theory, the model function in this work is $\varepsilon=\varepsilon_\infty+(\varepsilon_s-\varepsilon_\infty)/(1+\omega^2\tau^2)- i\ (\ (\varepsilon_s-\varepsilon_\infty)\ \omega\tau/(1+\omega^2\tau^2)+\sigma/(\omega\varepsilon_0))$, where ε_∞ is optical dielectric constant, ε_s is static dielectric constant, ε_0 is free space dielectric constant, τ is the relaxation time and σ is the conductivity.

To obtain ε_c'' *and* ε_p'', the ε_s, ε_∞, σ and τ should be fitted firstly, which are signed as a group β. The sum of squares is $S=\sum_{i=1}^{m} r_i^2$, where r_i presents $\varepsilon_{fit}-\varepsilon$. Our goal is minimizing the S by adjusting β. In order to fit these data as precise as possible, the original data are divided into twenty parts and fitted separately. The average value is used as the final result. As well, we use a Python package Scipy* to simplify our code.

```
import numpy as np
from scipy.optimize import least_squares
import xlrd

def realimag(array):
    return np.array([(x.real, -x.imag) for x in array])

def func(x,p):
    s,u,sigma,t=p                #s:static dielectric constant;u:optical dielectric constant;sigma:conductivity;t:relaxation time
    d=complex(0,1)
```

```
    o=8.854187817*10**(-12)
    return realimag( u+(s-u)/(1+x*x**t*t)
-np.dot(d,np.dot(np.dot(x,t),np.divide((s-u),(1+np.dot(np.dot(np.dot(x,x),t),t)))))
-np.dot(d,np.divide(sigma,np.dot(x,o)))      )

def condut_loss_result(x,p):
    s,u,sigma,t=p
    o=8.854187817*10**(-12)
    return np.divide(sigma,np.dot(x,o))

def residuals(p,y,x):
    return (realimag(np.array(y)) - func(x, p)).flatten()

p0 = [20,10,1,10**-12]
data=xlrd.open_workbook('original_data.xlsx')

data_number=200
groups=20


table=data.sheets()[3]
fcost=0
fsig=0                                          #fitting conductivity
ft=0                                            #fitting  relaxation
time
fplsq=[]
fs=0                                            #fitting  static
dielectric constant
```

```
fu=0                                                    #fitting optical
dielectric constant
fconduct_loss=0                                         #fitting conducting
loss
frelaxation_loss=0                                      #fitting polarization
loss
for i in range(1,int(groups)+1):

    end=i*(int(data_number/groups))
    start=end-int(data_number/groups)
    #print("Reading data group",i,": from ",start," to ",end)

    xdata=table.col_values(0)[start:end]
    ydata_1=table.col_values(2)[start:end]                  #imaginary
permitivity
    ydata_2=table.col_values(1)[start:end]                  #real permitivity
    ydata=[]



    for m in range(int(data_number/groups)):
        xdata[m]=xdata[m]*10**9                             # GHz
        ydata.append(complex(ydata_2[m],-ydata_1[m]))

    plsq = least_squares(residuals, p0,
bounds=([0,0,0,0],[200,200,200,10**-1]),args=(ydata, xdata),max_nfev=100000)
    fplsq.append(plsq)
    print(plsq.x[0],"  ",plsq.x[1],"  ",plsq.x[2],"  ",plsq.x[3],"  ")
    conduct_loss=np.mean(condut_loss_result(xdata,plsq.x))
```

```
    #print("Conduct_loss      ",i,":",conduct_loss)
    fconduct_loss += conduct_loss
    relaxation_loss=np.mean(ydata_1)-conduct_loss
    #print("Relaxation_loss",i,":",relaxation_loss)
    #print("Imaginary:",np.mean(ydata_1),",        Conduct        Loss:",conduct_loss,",
Relaxation Loss:",relaxation_loss)
    #print(np.mean(xdata)/10**9,"          ",np.mean(ydata_1),"          ",conduct_loss,"
",relaxation_loss)


    frelaxation_loss += relaxation_loss
    fsig=fsig+plsq.x[2]
    fs=fs+plsq.x[0]
    fu=fu+plsq.x[1]
    ft=ft+plsq.x[3]
    fcost=plsq.cost+fcost
```